



**HAL**  
open science

# Nature and evolution of the lithospheric mantle beneath the passive margin of East Oman: evidence from mantle xenoliths sampled by Cenozoic alkaline lavas

Michel Grégoire, Jessica Langlade, Guillaume Delpech, Céline Dantas,  
Georges Ceuleneer

## ► To cite this version:

Michel Grégoire, Jessica Langlade, Guillaume Delpech, Céline Dantas, Georges Ceuleneer. Nature and evolution of the lithospheric mantle beneath the passive margin of East Oman: evidence from mantle xenoliths sampled by Cenozoic alkaline lavas. *Lithos*, 2009, 112 (3-4), pp.203-216. 10.1016/j.lithos.2009.02.002 . hal-00535783

**HAL Id: hal-00535783**

**<https://hal.science/hal-00535783>**

Submitted on 12 Nov 2010

**HAL** is a multi-disciplinary open access archive for the deposit and dissemination of scientific research documents, whether they are published or not. The documents may come from teaching and research institutions in France or abroad, or from public or private research centers.

L'archive ouverte pluridisciplinaire **HAL**, est destinée au dépôt et à la diffusion de documents scientifiques de niveau recherche, publiés ou non, émanant des établissements d'enseignement et de recherche français ou étrangers, des laboratoires publics ou privés.

Elsevier Editorial System(tm) for Lithos  
Manuscript Draft

Manuscript Number:

Title: Nature and evolution of the lithospheric mantle beneath the passive margin of East Oman: evidence from mantle xenoliths sampled by Cenozoic alkaline lavas

Article Type: Research Paper

Section/Category:

Keywords: Oman; upper mantle; xenoliths; harzburgites; lherzolites; trace elements; metasomatism; Owen basin

Corresponding Author: Dr. Michel Gregoire, Ph.D.

Corresponding Author's Institution: CNRS-Observatoire Midi Pyrenees

First Author: Michel Gregoire, Ph.D.

Order of Authors: Michel Gregoire, Ph.D.; Michel Gregoire; Jessica Langlade; Guillaume Delpech; Celine Dantas; Georges Ceuleneer

Manuscript Region of Origin:

Abstract: Cenozoic alkaline lavas from the Al Ashkharah area, facing the Indian ocean along the North-East Oman coastline, contain numerous small (< 2cm) mantle xenoliths. They provide a unique opportunity to investigate the nature and evolution of the upper mantle beneath the Oman passive margin, bordering the Owen Basin. All studied xenoliths are porphyroclastic to equigranular spinel lherzolites and harzburgites. They are all devoid of amphibole and phlogopite. The composition of their clinopyroxenes, orthopyroxenes, olivines and spinels indicate that these samples are witnesses of a typical subcontinental lithospheric upper mantle and are quite distinct from the peridotites cropping out in the nearby Oman ophiolite.

The clinopyroxene major element composition record an evolution from fertile lherzolites (Mg#: 89 and Al<sub>2</sub>O<sub>3</sub>: 7.5 wt%) to refractory harzburgites (Mg#: 93.5 and Al<sub>2</sub>O<sub>3</sub>: 2.5 wt%). The clinopyroxene of most samples are characterised by REE patterns evolving continuously from spoon-shaped to LREE-enriched with almost flat HREE spectra (LaN/YbN: 2.5-30; LaN/SmN: 3.2-24; SmN/YbN: 0.25-4.6; HoN/LuN : 0.88-1.15) and strong negative Ba, Nb, Zr, Hf and Ti anomalies. We propose that these geochemical fingerprints can be accounted for in the frame of a two stages; (1) a - likely ancient - decompression melting event characterised by a degree ranging from 1 to a maximum of 19 % and unrelated to the recent tectonic evolution of the Oman margin, followed by (2) metasomatic transformation possibly related to the circulation of carbonate-rich silicate melt during the Cenozoic rifting event that led to the opening of the Owen basin.

1

2 **Nature and evolution of the lithospheric mantle beneath the passive**  
3 **margin of East Oman: evidence from mantle xenoliths sampled by**  
4 **Cenozoic alkaline lavas**

5

6

7 Grégoire<sup>1\*</sup>, M., Langlade<sup>1</sup>, J.A., Delpech, G.<sup>2</sup>, Dantas<sup>1</sup>, C. and Ceuleneer<sup>1</sup>, G.

8

9 1. CNRS-UMR 5562 DTP :Dynamique Terrestre et Planétaire. Observatoire Midi Pyrénées, Université  
10 Paul Sabatier,14 Avenue. E. Belin, 31400 Toulouse, France.

11 2. UMR CNRS 8148 IDES : Interactions et Dynamique des Environnements de Surface, Faculté des  
12 Sciences, Université Orsay-Paris Sud, Bât.504, 91405 ORSAY Cedex, France

13

14 • \* : Corresponding author : [michel.gregoire@ntp.obs-mip.fr](mailto:michel.gregoire@ntp.obs-mip.fr)

15 Tel: +33 5 61 33 29 77; Fax: +33 5 61 33 29 00

16

17

18

19

20

21

22

23

## 24 **Abstract**

25

26 Cenozoic alkaline lavas from the Al Ashkharah area, facing the Indian ocean along  
27 the North-East Oman coastline, contain numerous small (< 2cm) mantle xenoliths.  
28 They provide a unique opportunity to investigate the nature and evolution of the  
29 upper mantle beneath the Oman passive margin, bordering the Owen Basin. All  
30 studied xenoliths are porphyroclastic to equigranular spinel lherzolites and  
31 harzburgites. They are all devoid of amphibole and phlogopite. The composition of  
32 their clinopyroxenes, orthopyroxenes, olivines and spinels indicate that these  
33 samples are witnesses of a typical subcontinental lithospheric upper mantle and are  
34 quite distinct from the peridotites cropping out in the nearby Oman ophiolite.

35 The clinopyroxene major element composition record an evolution from fertile  
36 lherzolites (Mg#: 89 and Al<sub>2</sub>O<sub>3</sub>: 7.5 wt%) to refractory harzburgites (Mg#: 93.5 and  
37 Al<sub>2</sub>O<sub>3</sub>: 2.5 wt%). The clinopyroxene of most samples are characterised by REE  
38 patterns evolving continuously from spoon-shaped to LREE-enriched with almost flat  
39 HREE spectra (La<sub>N</sub>/Yb<sub>N</sub>: 2.5-30; La<sub>N</sub>/Sm<sub>N</sub>: 3.2-24; Sm<sub>N</sub>/Yb<sub>N</sub>: 0.25-4.6; Ho<sub>N</sub>/Lu<sub>N</sub> : 0.88-  
40 1.15) and strong negative Ba, Nb, Zr, Hf and Ti anomalies. We propose that these  
41 geochemical fingerprints can be accounted for in the frame of a two stages; (1) a -  
42 likely ancient - decompression melting event characterised by a degree ranging from  
43 1 to a maximum of 19 % and unrelated to the recent tectonic evolution of the Oman  
44 margin, followed by (2) metasomatic transformation possibly related to the circulation  
45 of carbonate-rich silicate melt during the Cenozoic rifting event that led to the  
46 opening of the Owen basin.

47

48

## 49 Key words

50 Oman; upper mantle; xenoliths; harzburgites; lherzolites; trace elements;  
51 metasomatism; Owen basin.

52

## 53 Introduction

54 Mantle xenoliths brought to the surface by alkaline magmas provide a direct  
55 access to the petrological processes conditioning the nature and evolution of the  
56 upper mantle (e.g. Coltorti et al., 1999 ; Grégoire et al., 1997 and 2000 ; Delpech et  
57 al., 2004). Mantle xenoliths from continental rift systems have been largely studied all  
58 around the world in the last decades (e.g. Ionov et al., 2002; Witt-Eickschen et al.,  
59 2003 ; Lenoir et al., 2000). Small (< a few cm), mostly lherzolitic, xenoliths have  
60 been recently discovered in alkaline dykes and flows emplaced during Cenozoic  
61 times along the Oman passive margin facing the Owen basin (see Gnos and Peters,  
62 2003) but they have not been extensively studied yet for their trace element  
63 geochemistry. Nasir et al. (2006) report on bulk rock trace element analyses but,  
64 given the small size of the xenoliths, contamination with the host lava cannot be  
65 excluded. Among other, the marked enrichment in incompatible elements they  
66 observed might not be related to mantle processes. The present paper is a  
67 complementary study to the one of these authors in terms of analytical procedure: we  
68 performed *in situ* (LA-ICP-MS) determinations of the trace element content of  
69 clinopyroxene to avoid at best the risk of contamination with the host alkaline lavas.  
70 Moreover, we sampled some localities not studied by Nasir et al. (2006) and the  
71 lithological diversity of our collection appears to be more pronounced. The question  
72 addressed in the present paper concerns the nature of the upper mantle beneath the

73 eastern Oman mountains, among other how does it compare to the peridotites  
74 cropping out in the Semail ophiolite, relics of the sub-oceanic mantle from a nearby  
75 area. Our aim is also to decipher if the upper mantle beneath the Oman margin was  
76 affected by the melting and/or melt migration processes related to the Cenozoic  
77 rifting of the Owen basin. We compare our results to those from the studies of the  
78 mantle peridotite xenoliths from Spitsbergen (Ionov et al., 2002; Gregoire et al.,  
79 submitted). Indeed the latter come from the same kind of setting (rift-zones) and  
80 display close similarities with the xenoliths studied here.

81

## 82 Geological setting and sampling

83

84 The building and present structure of the Northern Oman mountains result essentially  
85 from the obduction of the Semail ophiolite during Maestrichtian times and from a  
86 regional uplift that started during the Miocene (Glennie et al, 1974; Coleman, 1981).  
87 Our study area is located at the eastern termination of this domain, along a major  
88 structural lineament referred to as the Masirah fault (Moseley, 1969). The Masirah  
89 line acted as a major transform plate boundary that accommodated the northward  
90 drift of the Indian continental block during Cretaceous and Paleocene times (e.g.  
91 Royer et al, 2002; Fournier et al, 2008). As a result of the kinematic reorganization  
92 that followed the India-Eurasia collision (about 52 Ma ago, Patriat and Achache,  
93 1984), this transform boundary shifted into its present “off shore” position along the  
94 Owen Fracture Zone.

95 Although this general picture is reasonably well understood, the precise evolution of  
96 the Eastern Oman margin during the late Cretaceous and early Cenozoic times was  
97 rather complex and is still poorly constrained. Regional geological studies have

98 shown that long transtensive periods alternated with shorter transpressive ones (e.g.  
99 Platel and Roger, 1989). The best documented of these transpressive “events”  
100 occurred during upper Maastrichtian lower Paleocene times; it is witnessed by the  
101 oblique thrusting of sedimentary nappes and by the obduction of the Masirah  
102 ophiolite, a piece of upper Jurassic oceanic lithosphere that likely evolved in a ridge-  
103 transform tectonic setting during the accretion of the proto-Indian ocean (Gnos and  
104 Perrin, 1995; Gnos et al, 1997; Peters and Mercogli, 1998). Since Eocene times, the  
105 coast of East Oman behaved like a passive margin bordering a rift zone that  
106 eventually led to the opening of the Gulf of Aden (Platel and Roger, 1989). The  
107 opening of the Owen basin is possibly one of the events that complicated the  
108 evolution of this margin, although the age of the oceanic crust in the Owen basin is  
109 still debated (Fournier et al, 2008). Current structural and kinematic studies, among  
110 other around the Aden-Owen-Carlsberg triple junction will result in a better  
111 understanding of the evolution of this area (J.-Y. Royer, pers. com.).

112 Alkaline magmatism that affected the East Oman margin seems to belong to two  
113 main eruptive events: a first one contemporaneous with the compressive stage that  
114 affected the area at the Cretaceous-Tertiary boundary, and more recent dyke  
115 injections during the Eocene extension.

116 Mantle xenoliths studied in the present study were sampled in five occurrences of  
117 these N-S to NNE-SSW trending tertiary dykes in the Al Ashkarah area (Figure 1).  
118 Their precise age is poorly constrained: the dykes cross-cut Paleocene sediments  
119 but not more recent Eocene ones. Ar/Ar ages ranging from about 36 to 40 Ma have  
120 been published by Worthing and Wilde (2002) for the dykes including our samples of  
121 mantle xenoliths showing that they belong to the second, Eocene, injection event.

122

## 123 **Analytical methods**

124

125 Major and trace elements of minerals were analysed at the UMR 5563 (LMTG,  
126 Observatoire Midi-Pyrénées) of University Paul Sabatier (Toulouse III).

127 Major-element compositions of minerals were determined with the CAMECA SX50  
128 electron microprobe and a standard program: beam current of 20nA and acceleration  
129 voltage of 15 kV, 10 to 30s/peak, 5-10s/background counting times, and natural and  
130 synthetic minerals as standards. Nominal concentrations were subsequently  
131 corrected using the PAP data reduction method (Pouchou and Pichoir, 1984). The  
132 theoretical lower detection limits are about 100 ppm (0,01%).

133 The concentrations of Rare Earth Elements and other trace elements (La, Ce, Pr, Nd,  
134 Sm, Eu, Gd, Tb, Dy, Ho, Er, Yb, Lu, Rb, Ba, Th, Sr, Zr, Ti, Y, Ni, V and Sc) in  
135 clinopyroxenes were analysed in situ on >120  $\mu\text{m}$  thick polished sections with a  
136 Perkin-Elmer Elan 6000 ICP-MS instrument coupled to a CETAC laser ablation  
137 module that uses a 266 nm frequency-quadrupled Nd-YAG laser. The NIST 610 and  
138 612 glass standards were used to calibrate relative element sensitivities for the  
139 analyses. The analysis were normalized using CaO values determined by electron  
140 microprobe. The analyses were performed on inter-clivage area from the cores of the  
141 freshest cpx grains in order to get homogeneous results unaffected by alteration or  
142 exsolution processes. A beam diameter of 50-100  $\mu\text{m}$  and a scanning rate of 20  $\mu\text{m}/\text{s}$   
143 were used. The typical relative precision and accuracy for a laser analysis range from  
144 1 to 10%. Typical theoretical detection limits range from 10 to 20 ppb for REE, Ba,  
145 Rb, Th, Sr, Zr and Y; 100ppb for Sc and V; and 2 ppm for Ti and Ni (see in Dantas et  
146 al., 2007 for more details).

147



## 148 **Petrography**

149

150 The lavas hosting the ultramafic xenoliths are microlitic basalts. The xenoliths being  
151 small, < 2cm in size (Figure 2), it has been difficult to define the rock-types  
152 unambiguously. Nevertheless, we distinguished two main rock types: (i) spinel  
153 lherzolites (samples 04OM58a2, 04OM58a3, 04OM58c3, 04OM58f3, 04OM59b2,  
154 04OM62b2, 04OM63c2, and 04OM66d2); and (ii) spinel harzburgites (samples  
155 04OM58b1, 04OM62b1, 04OM63a1, 04OM63a2, 04OM63c1 and 04OM63c3). None  
156 of the xenoliths display amphibole or phlogopite. All the peridotites correspond to  
157 mantle peridotites equilibrated in the spinel stability field. Considering the small size  
158 of the xenoliths, the following modal compositions are only indicative.

159         The peridotites are relatively fresh, the serpentinisation of the olivine and the  
160 orthopyroxene being always limited. Some clinopyroxenes and particularly those  
161 from sample 04OM62b2, show spongy textures commonly limited to the rim but  
162 sometimes affecting the entire crystal. The formation of this type of texture is  
163 probably related to local melting process affecting the clinopyroxenes during the  
164 transport of the xenoliths to the surface by the host-lavas (e.g. Grégoire et al., 2000,  
165 Carpenter et al., 2002).

166         Orthopyroxenes commonly contains thin lamellae of exsolved clinopyroxene.  
167 The inverse phenomenon occurs but is less common. Orthopyroxene also contains  
168 tiny inclusions of spinel. The cleavage in the pyroxenes from the sample 04OM63a1  
169 and 04OM63a2 are clearly bent and sometimes the pyroxenes are fractured while  
170 olivines display undulose extinction (Figure 2). Within those fractures some neoblasts  
171 of clinopyroxene and orthopyroxene appear. This can be attributed to a deformation

172 process undergone by the samples within the upper mantle (e.g. Mercier and  
173 Nicolas, 1975).

174 The lherzolites have porphyroclastic or equigranular textures. Their modal  
175 compositions roughly range from 10 to 20% of clinopyroxene, 60 to 85% of olivine,  
176 10 to 30% of orthopyroxene, and <10% of spinel. The olivine and pyroxenes  
177 porphyroclasts can reach 4mm in size while the neoblasts are typically less than 0.5  
178 mm in size. Spinel size ranges from a few microns to 1 mm. The spinels are  
179 generally interstitial or in inclusion in olivine and clinopyroxene (Figure 2).

180 The harzburgites commonly display porphyroclastic or equigranular textures and  
181 more rarely a protogranular one. Their modal composition ranges from 55 to 70% of  
182 olivine, 30 to 40% of orthopyroxene, and close to 5% of clinopyroxene and spinel.  
183 The olivine and orthopyroxene porphyroclasts can reach 8 mm in size while the  
184 neoblasts are always < 0.5 mm in size. Clinopyroxene is interstitial and commonly  
185 less than 1-2 mm in size. Spinel commonly occur as tiny inclusions (<1 mm) in the  
186 silicates or as vermicular interstitial slightly bigger crystals (1-2 mm).

187

## 188 **Mineral composition:**

### 189 ***Olivine, Orthopyroxene and Spinel (Table 1)***

190 Olivine is the dominant mineral phase in all samples. Olivines in harzburgites  
191 and lherzolites are very magnesian with their Mg-number ( $100 \cdot \text{Mg}/\text{Mg} + \text{Fe}_{\text{total}}$ )  
192 ranging from 89 to 91.2. Olivines of harzburgites are commonly more magnesian  
193 than those of lherzolites. Olivine has low CaO (<0.15 wt.%), MnO (< 0.25 wt.%) and  
194  $\text{Cr}_2\text{O}_3$  (< 0.07 wt.%) contents and NiO contents ranging from 0.25 to 0.54 wt. %.

195 Orthopyroxenes show the same compositional range as olivines with Mg-  
196 number ( $100 \cdot \text{Mg}/\text{Mg} + \text{Fe}_{\text{total}}$ ) varying from 89.5 to 92. The  $\text{Al}_2\text{O}_3$  content of

197 orthopyroxene ranges from 2 to 5.5 wt. % and TiO<sub>2</sub> content is always very low (<0.15  
198 wt. %). The Cr<sub>2</sub>O<sub>3</sub> and CaO content ranges from 0.3 to 0.75 wt. % and 0.7 to 1.2 wt.  
199 %, respectively. It has to be noticed that the Iherzolite 04OM62b2 and the harzburgite  
200 04OM64b1 display the more aluminous (5.5 wt %) and titaniferous (0.15 wt%) and  
201 the less aluminous (2 wt%), more chromiferous (0.75 wt%) and magnesian (Mg-  
202 number: 92) orthopyroxene, respectively.

203 Most spinels are relatively unzoned magnesian and aluminous chromites with  
204 Mg-number and Cr-number (100\*Cr/Cr+Al) ranging from 70 to 80 and from 16 to  
205 19.5, respectively. However, spinels of two samples are out of this Cr-number range.  
206 The harzburgite 04OM62b1 and the Iherzolite 04OM62b2 respectively contain a  
207 more and a less chromiferous spinel (Cr# = 60 and 11.2), the former being also a  
208 little bit less magnesian (Mg# =64.4). In a Cr-number vs. Mg-number diagram (Figure  
209 3), spinels plot in the field defined by spinels from the mantle peridotitic xenoliths  
210 from Spitsbergen, which is also a continental rifting area (Ionov et al., 2002). They  
211 are also similar to the spinels of the Oman mantle xenoliths studied by Nasir et al.  
212 (2006) but different from those of the mantle section of the Oman ophiolite (Figure 3).

213

#### 214 ***Clinopyroxene :***

##### 215 Major elements (Table 1)

216 Clinopyroxenes are commonly diopsides but in samples 04OM62b1 and 04OM62b2  
217 where they are Mg-augites. The clinopyroxene major element compositions highlight  
218 an evolution from fertile Iherzolites (sample 04OM62b2: Mg#: 88.8 and Al<sub>2</sub>O<sub>3</sub>: 7.5  
219 wt% to refractory harzburgites Mg#: 93.8 and Al<sub>2</sub>O<sub>3</sub>: 2.5 wt%). Cr<sub>2</sub>O<sub>3</sub> and TiO<sub>2</sub>  
220 contents of most samples are relatively homogeneous, varying respectively from 0.3  
221 to 1 wt% and from 0 to 0.2 wt%. However, the Cr<sub>2</sub>O<sub>3</sub> content (up to 1.6 wt%) of the

222 clinopyroxenes from the harzburgite 04OM62b2 and the  $Ti_2O$  content of  
223 clinopyroxenes of the lherzolite 04OM62b2 (0.5 wt. %) are higher. Finally  $Na_2O$   
224 content of clinopyroxenes of both types of peridotite ranges from 0.4 to 1.4 wt%. In  
225 Figure 4 the clinopyroxenes display a range of composition similar to that defined by  
226 the clinopyroxenes from mantle peridotitic xenoliths from Spitsbergen. The  
227 clinopyroxenes of harzburgites have the same  $Al_2O_3$  contents than that of the  
228 clinopyroxenes from the mantle peridotites of the Oman ophiolite (Monnier et al.,  
229 2006) but have higher  $Na_2O$  contents and commonly lower  $Cr_2O_3$  contents (Figure 4).  
230 Finally, the clinopyroxenes of the mantle xenoliths from Oman studied by Nasir et al.  
231 (2006) display intermediate compositions between those of the studied lherzolites  
232 and those of the studied harzburgites.

233

#### 234 Trace elements

235 Trace element abundances of clinopyroxenes are given in Table 2. The REE  
236 contents of clinopyroxenes of most of the studied harzburgites and lherzolites are  
237 characterised by similar patterns evolving almost regularly from spoon-shaped  
238 patterns to LREE-enriched patterns characterised by an almost HREE-flat shape  
239 ( $La_N/Yb_N$ : 2.5-30;  $La_N/Sm_N$ : 3.2-24;  $Sm_N/Yb_N$ : 0.25-4.6;  $Ho_N/Lu_N$  : 0.88-1.15; Figure 5).  
240 These clinopyroxenes also display similar trace element patterns characterised by  
241 strong negative Ba, Nb, Zr, Hf and Ti anomalies. They appear to be similar to those  
242 of mantle peridotite xenoliths in alkaline lavas from Spitsbergen which have been  
243 subdivided into two types: the type-1 is characterized by spoon-shaped REE patterns  
244 and the type-2 displays LREE-enriched patterns (Ionov and al., 2002, Figure 5).  
245 Only the lherzolite 04OM62b2 and the harzburgite 04OM62b1 display different REE  
246 patterns, being LREE-depleted ( $La_N/Yb_N$ : 0.29;  $La_N/Sm_N$ : 0.35;  $Sm_N/Yb_N$ : 0.82;

247  $\text{Ho}_N/\text{Lu}_N$ : 1.16) and LREE-enriched with HREE fractionation ( $\text{La}_N/\text{Yb}_N$ : 9.32;  $\text{La}_N/\text{Sm}_N$ :  
248 1.52;  $\text{Sm}_N/\text{Yb}_N$ : 6.14;  $\text{Ho}_N/\text{Lu}_N$ : 2.99), respectively (Figure 6). The clinopyroxene trace  
249 element pattern of the lherzolite 04OM62b2 displays negative Nb and Ti anomalies  
250 and a slight positive Sr anomaly while that of the harzburgite 04OM62b1 shows  
251 negative Ba, Nb, Zr, Hf and Ti anomalies and a similar slight positive Sr anomaly  
252 (Figure 6).

253

## 254 **Discussion**

255

256 The studied suite of mantle xenoliths included in the alkaline lavas from the Al  
257 Ashkharah region in Oman is composed lherzolites and harzburgites last equilibrated  
258 within the mantle spinel peridotite stability field. We estimate their temperatures of  
259 equilibration within the spinel stability field by using the geothermometers of Wells  
260 (1977) and Brey and Kohler (1990), both based on the orthopyroxene/clinopyroxene  
261 pair. Irrespective of the lithology (lherzolite and harzburgite), the temperature  
262 estimates all range between 900 and 1150 °C using the calibration by Wells and  
263 between 850 °C and 1160 °C (at P: 1.5 GPa) with that of Brey and Kohler.

264 The fact that we found only spinel harzburgites and lherzolites in the present  
265 study appears to be a main difference with the study of Nasir et al. (2006), who  
266 describe spinel wehrlites and dunites in their suite of mantle xenoliths from the Al  
267 Ashkharah area and spinel wehrlites, lherzolites and dunites in their mantle xenolith  
268 suite from Muscat area (Figure 1). In both cases the sample sizes are very small ( $\leq$   
269 2cm in size) and therefore the modal estimates need to be taken with caution. Our  
270 suite of samples is very close in terms of petrographic diversity to the mantle  
271 xenoliths (harzburgites and lherzolites) from Spitsbergen (Ionov et al., 2002) as far as

272 peridotites are concerned. In the other hand they appear very different in term of  
273 petrographic diversity and mineral compositions from the mantle peridotites from the  
274 Oman ophiolite (mostly harzburgites and dunites in the ophiolite) (Figures 3, 4 and  
275 8).

276 Most samples studied in the present study present several characteristics of  
277 solid residues resulting from partial melting, including high Mg number of olivine and  
278 pyroxenes, high Cr<sub>2</sub>O<sub>3</sub> content of spinel. The HREE patterns of the clinopyroxenes  
279 are also in agreement with such a process (Figure 5). In order to estimate the degree  
280 of partial melting experienced by the Oman upper mantle we used two methods: (i)  
281 Firstly, we estimated the degree of partial melting by using the Cr# of spinel following  
282 the method of Hellebrand et al. (2001) calibrated for Cr# values in spinel ranging  
283 between 0.10 and 0.60, a range similar to that of our samples. The results mostly  
284 range from 2 to 8 % except for the harzburgites 04OM58b1 and 04OM62b1 that give  
285 estimates of 13 and 19 %, respectively. (ii) Secondly, we compared the REE  
286 contents of the clinopyroxenes with those computed using a model of fractional  
287 melting for a primitive spinel-peridotite mantle source, based on the method  
288 described by Johnson et al. (1990) (Figure 7). The starting composition and melting  
289 modes are those given by Hellebrand et al., (2002). In Figure 7 the REE from Dy to  
290 Yb are in good agreement with the partial melting model. The estimated degrees of  
291 melting using the HREE (Dy-Yb), which are the least subjected to metasomatism,  
292 range from 1 to about 6 % (Figure 7). This is with the exception of the harzburgite  
293 04OM62b1, for which the partial melting modelling indicates inconsistent partial  
294 melting degrees between 10% (for Er) and 15% (for Yb). This is not plausible if we  
295 consider melting in the stability field of spinel because Er and Yb have very similar  
296 partition coefficients, such as in the present model. The MREE and HREE contents

297 of the clinopyroxene in harzburgite 04OM62b1 could also indicate that the  
298 clinopyroxenes in this xenolith were in equilibrium with garnet because of the higher  
299 partition coefficients for HREE in garnet. Moreover, the LREE and MREE from La to  
300 Gd do not match the partial melting modelling. The clinopyroxenes have LREE and  
301 MREE that are more enriched than predicted from the partial melting modelling.  
302 These enrichments in LREE and MREE most probably reflect processes that  
303 occurred after the partial melting event (see below). Finally in the harzburgite  
304 04M62b1 the best estimate of the partial melting degree is given by the Cr# of spinel  
305 using the method of Hellebrand et al. (2002), i.e. a degree close to 19%.

306 In the other hand, beside the evidence for partial melting processes (see  
307 above) the majority of the studied Oman spinel peridotite xenoliths display evidence  
308 for mantle metasomatism. This is supported by the concomitant increase of the Na  
309 and Cr contents of clinopyroxenes (Figure 8). the REE patterns of most of the  
310 clinopyroxenes (spoon-shaped and LREE-enriched) and the enrichment in the most  
311 incompatible elements (Th, U, Sr), that point out to mantle metasomatism. The  
312 selective enrichments in the most incompatible elements, LREE and MREE in mantle  
313 clinopyroxenes are widely accepted to be the result of the infiltration of a fluid or of a  
314 melt into the mantle rocks (e.g. O'Reilly and Griffin, 1988; Coltorti et al., 1999; Van  
315 Achterberg et al., 2001; Grégoire et al., 2003 and 2005). The fact that only the most  
316 incompatible trace elements (Th, U, Sr, LREE) are enriched in numerous samples is  
317 in agreement with the percolation of a metasomatic agent at low melt/rock ratio. Thus  
318 it appears that the studied mantle xenoliths from Oman record two types of  
319 processes : partial melting and metasomatism.

320 Most of the clinopyroxenes from the mantle peridotites from the Al Ashkharah  
321 area display REE patterns similar to those of the mantle spinel peridotite xenoliths

322 entrained by the alkaline lavas from Spitsbergen (Ionov et al., 2002 a and b; Figure  
323 6). Ionov et al. (2002) proposed a two-stage evolution model to explain the history of  
324 xenoliths from Spitsbergen. First partial melting of a more or less fertile peridotitic  
325 mantle (degree of partial melting up to 22% for the most refractory samples), which  
326 formed residues characterized by LREE-depleted patterns. These melting residues  
327 were subsequently metasomatised by OIB-like carbonate-rich mafic silicate melts  
328 (Ionov et al., 2002 a and b). This metasomatic event led to the re-enrichment in the  
329 most incompatible elements and LREE ( $\pm$ MREE) in the clinopyroxenes such as in  
330 Figure 6. If we compare the Spitsbergen mantle clinopyroxenes with the studied  
331 Oman mantle clinopyroxenes, the later display very similar REE and incompatible  
332 trace element patterns (Figure 5) and therefore it is plausible that the metasomatic  
333 agents are similar in composition in the two cases. Finally the same two-stage  
334 evolution model can be invoked to explain the trace element compositions of most  
335 samples from this study. The studied mantle xenoliths from Al Ashkarah have been  
336 affected in a first stage by partial melting degrees between 1 to a maximum of 19 %.  
337 Later, in a second stage, the melting residues have suffered a metasomatic event  
338 leading to the re-enrichment in the most incompatible elements and LREE ( $\pm$ MREE)  
339 of the clinopyroxenes in the Iherzolites, but also of the MREE  $\pm$  HREE in the  
340 harzburgites, which are more sensitive to metasomatism. The metasomatic agent is  
341 probably a carbonate-rich mafic silicate melt enriched in highly incompatible trace  
342 elements and characterised by low abundances of Nb, Zr, Hf and Ti. Such  
343 characteristics allow to propose the hypothesis of a link between this metasomatic  
344 melt and the OIB-like tertiary alkaline melts of the same area including the host lavas  
345 of mantle xenoliths studied by Worthing and Wilde (2002) and Nasir et al. (2006).  
346 This link is strengthened by the similarity of trace element patterns of the calculated



347 liquids in equilibrium with the clinopyroxenes of samples 04OM62b1 and OM63c1  
348 with that of the host lava (Figure 9). For that calculation we used the  
349 clinopyroxene/basanite partition coefficients at 0.5 GPa from Adam and Green  
350 (2003). In such a model, the clinopyroxenes of samples 04OM62b2 (Lherzolite) and  
351 04OM62b1 (Harzburgite) characterized by respectively a LREE-depleted REE  
352 pattern and a LREE-enriched one characterised by HREE fractionation may  
353 represent: (i) a witness of the first stage of the model (sample 04OM62b2), i.e. the  
354 process of partial melting or even the upper mantle before the partial melting as the  
355 clinopyroxene of this sample displays a REE pattern similar to that of the estimated  
356 primitive upper mantle (Figure 7) and (ii) a crystallization product of the metasomatic  
357 carbonate-rich silicate melt. Indeed the latter displays some similarities with the  
358 sample 4-90-1 from Ionov et al. (2002) which is a composite xenolith consisting of an  
359 amphibole-bearing wehrlite grading to an olivine-dominated zone with clusters of  
360 amphiboles. That sample is a fragment of a magmatic vein within the peridotitic  
361 mantle, a vein formed by a melt displaying similar REE content than that of the  
362 metasomatic agent responsible of the incompatible trace element enrichment of the  
363 Spitsbergen mantle xenoliths (Ionov et al., 2002).

364

## 365 **Summary**

366 The upper mantle equilibrated in the spinel stability field beneath the North West Al  
367 Ashkharah (East Oman) area mostly consists of lherzolites and harzburgites. This  
368 region of the upper mantle has been affected by two main petrogenetic processes: (i)  
369 an early partial melting event mostly of low degree leading to the formation of a  
370 LREE-depleted clinopyroxene in the peridotitic mantle residue and (ii) a metasomatic  
371 event linked to the circulation within this previously slightly depleted upper mantle of

372 a OIB-like carbonate-rich mafic silicate melt. The upper mantle beneath the North  
373 West Al Ashkharah therefore has a similar history than that of the upper mantle  
374 beneath Spitsbergen, an other continental rifting area. We tentatively suggest that  
375 the partial melting event is an old event while the metasomatic melt is related to the  
376 tertiary alkaline magmatic activity of the studied area related to the rifting of the  
377 Oman passive margin that led to the opening of the Owen basin

378

379

## 380 **ACKNOWLEDGMENTS**

381

382 We warmly thank M. Monnereau for his help on the field and H. Al Azri from the  
383 Ministry of Commerce and Industry of Oman for constant support. Thin sections,  
384 electron microprobe analyses and ICP-MS analyses were performed using the  
385 facilities of the Observatoire Midi-Pyrénées, Paul Sabatier University, Toulouse. We  
386 are particularly indebted to F. de Parseval and J.-F. Mena for thin and thick section  
387 preparation, P. de Parseval for his help during microprobe data acquisition and F.  
388 Candaudap and R. Freydier for their help during LA-ICPMS data acquisition. This  
389 work was financially supported by the French Centre National de la Recherche  
390 Scientifique.

391

## 392 **REFERENCES**

393

394 Adam, J., Green, T., 2003. The influence of pressure, mineral composition and water  
395 on trace element partitioning clinopyroxene, amphibole and basanitic melts.  
396 European Journal of Mineralogy 15, 831-841.

397

398 Brey, G.P., Kohler, T., 1990. Geothermobarometry in four-phase lherzolites II. New  
399 thermobarometers, and practical assessment of existing thermobarometers. *Journal*  
400 *of Petrology* 31, 1353-1378.  
401

402 Carpenter, R.L., Edgar, A.D., Thibault. 2002. Origine of spongy textures in  
403 clinopyroxene and spinel from mantle xenoliths, Hessian Depression, Germany.  
404 *Mineralogy and Petrology* 74: 149-162.  
405

406 Coleman, R.G., 1981. Tectonic setting for ophiolite obduction in Oman. *Journal of*  
407 *Geophysical Research* 86, 2497-2508.  
408

409 Coltorti, M., Bonadiman, C., Hinton, R.W., Siena, F., Upton, B.G.J., 1999.  
410 Carbonatite metasomatism of the oceanic upper mantle: evidence from  
411 clinopyroxenes and glasses in ultramafic xenoliths of Grande Comore, Indian Ocean.  
412 *Journal of Petrology* 40, 133-165.  
413

414 Dantas, C., Ceuleneer, G., Grégoire, M., Python, M., Freydier, R., Warren, J., Dick  
415 H.B.J., 2007. Pyroxenites dredged along the south-west Indian Ridge, 9°-16°E:  
416 cumulates from incremental melt fractions produced at top of a cold melting regime.  
417 *Journal of Petrology* 48, 647-660.  
418

419 Delpech, G., Grégoire, M., O'Reilly, S.Y., Cottin, J.Y., Moine, B.N., Michon, G. 2004.  
420 Feldspar from carbonate-rich metasomatism in the oceanic mantle under Kerguelen  
421 Islands (South Indian Ocean), *Lithos* 75, 209-237.  
422

423 Fournier, M., Chamot-Rooke, N., Petit, C., Fabbri, O., Huchon, P., Maillot, B.,  
424 Lepvrier C., 2008. In situ evidence for dextral active motion at the Arabia-India plate  
425 boundary. *Nature Geosciences* 1, 54-58.  
426

427 Glennie, K.W., Boeuf, M.G.A., Hughes-Clark, M.W., Moody-Stuart, M., Pilaar, W.F.H.,  
428 Reinhardt, B.M., 1974. Geology of the Oman mountains. *Verhandling Koninkelijk*  
429 *Nederlands Geologisch Mijnboukundig Genootschap* 31, 423 pp.  
430

431 Gnos, E., Immenhauser, A., Peters T., 1997. Late Cretaceous/Early Tertiary  
432 convergence between the Indian and Arabian plates recorded in ophiolites and  
433 related sediments. *Tectonophysics* 271, 1-19.  
434

435 Gnos, E., Perrin, M., 1995. Formation and evolution of the Masirah ophiolite  
436 constrained by paleomagnetic study of volcanic rocks. *Tectonophysics* 253, 53-64.  
437

438 Gnos, E., Peters, T., 2003. Mantle xenolith-bearing Maastrichtian to Tertiary alkaline  
439 magmatism in Oman. *Geochemistry, Geophysics, Geosystems (G-cubed)* 4, 8620,  
440 doi: 10.1029/2001GC000229.  
441

442 Grégoire, M., Lorand, J.P., Cottin, J.Y., Giret, A., Mattielli, N., Weis, D., 1997.  
443 Petrology of Kerguelen mantle xenoliths: Evidence of a refractory oceanic mantle  
444 percolated by basaltic melts beneath the Kerguelen archipelago. *European Journal of*  
445 *Mineralogy* 9, 1085-1100.  
446

447 Grégoire, M., Moine, B.N., O'Reilly, S.Y., Cottin, J.Y., Giret, A., 2000. Trace element  
448 residence and partitioning in mantle xenoliths metasomatized by highly alkaline,  
449 silicate- and carbonate-rich melts Kerguelen Islands, Indian Ocean. *Journal of*  
450 *Petrology* 41, 477-509.  
451

452 Grégoire, M., Bell, D.R., Le Roex, A.P., 2003. Garnet lherzolites from the Kaapvaal  
453 craton South Africa: trace elements evidence for a metasomatic history. *Journal of*  
454 *Petrology* 44, 629-657.  
455

456 Grégoire, M., Tinguely, C., Bell, D.R., Le Roex, A.P., 2005. Spinel lherzolite xenoliths  
457 from the Premier kimberlite (Kaapvaal craton, South Africa): Nature and evolution of  
458 the shallow upper mantle beneath the Bushveld complex. *Lithos* 84, 185-205.  
459

460 Grégoire, M., Chevet, J., Maaloe, S. Composite xenoliths from Spitsbergen: evidence  
461 of the circulation of MORB-related melts within the upper mantle. Submitted to  
462 *Geological Society of London special publication*.  
463

464 Hellebrand, E., Snow, J.E., Dick, H.J.B., Hofmann, A., 2001. Coupled major and  
465 trace elements as indicators of the extent of melting in mid-ocean-ridge peridotites.  
466 Nature 410, 677-681.

467

468 Hellebrand, E., Snow, J.E., Hoppe, P., Hofmann, A., 2002. Garnet-field melting and  
469 late-stage refertilization in "residual" abyssal peridotites from the Central Indian  
470 Ridge. Journal of Petrology 43, 12, 2305-2338.

471

472 Ionov, D. A., Bodinier, J. L., Mukasa, S. B., Zanetti, A., 2002a. Mechanisms and  
473 sources of mantle metasomatism: major and trace element compositions of peridotite  
474 xenoliths from Spitsbergen in the context of Numerical Modelling. Journal of  
475 Petrology 43, 2219-2259.

476

477 Ionov, D. A., Mukasa, S. B., Bodinier, J. L., 2002b. Sr-Nd-Pb isotopic compositions.  
478 of peridotite xenoliths from Spitsbergen. Numerical Modelling indicates Sr-Nd  
479 decoupling in the mantle by melt percolation processes. Journal of Petrology 43,  
480 2261-2278.

481

482 Johnson, K.T. M., Dick, H. J. B., Shimizu, N., 1990. Melting in the oceanic upper  
483 mantle: an ion microprobe study of diopsides in abyssal peridotites. Journal of  
484 Geophysical Research 95, 2661-2678.

485

486 Lenoir, X., Garrido, C.J., Bodinier, J.-L., Dautria, J.-M., 2000. Contrasting lithospheric  
487 mantle domains beneath the Massif Central (France) revealed by geochemistry of  
488 peridotite xenoliths. Earth and Planetary Science Letters 181, 359-375.

489

490 McDonough, W. F., Sun, S., 1995. The composition of the Earth. Chemical Geology  
491 120, 223-253.

492

493 Mercier, J-C. C., Nicolas, A., 1975. Textures and fabrics of upper-mantle peridotites  
494 as illustrated by xenoliths from basalts. Journal of Petrology 16, 454-487.

495

496 Monnier, C., Girardeau, J., Le Mée, L., Polvé, M. 2006. Along-ridge petrological  
497 segmentation of the mantle in the Oman ophiolite. *Geochemistry, Geophysics,*  
498 *Geosystems (G-cubed)* 7, Q11008, doi: 10.1029/2006GC001320.

499

500 Moseley, F., 1969. The upper cretaceous ophiolite complex of Masirah island, Oman.  
501 *Geological Journal*, 6, 293-306.

502

503 Nasir, S., Al-Sayigh, A., Alharthy, A., Al-Lazki, A., 2006. Geochemistry and petrology  
504 of Tertiary volcanic rocks and related ultramafic xenoliths from the central and  
505 eastern Oman Mountains. *Lithos* 90, 249–270

506

507 O'Reilly, S.Y., Griffin, W.L., 1988. Mantle metasomatism beneath Victoria, Australia I:  
508 metasomatic processes in Cr-diopside lherzolites. *Geochimica et Cosmochimica*  
509 *Acta* 52, 433– 447.

510

511 Patriat, P., Achache, J., 1984. India-Eurasia collision chronology has implications for  
512 crustal shortening and driving mechanisms of plates. *Nature* 311, 615-621.

513

514 Peters, T., Mercolli, I., 1998. Extremely thin oceanic crust in the Proto-Indian Ocean:  
515 evidence from the Masirah ophiolite, Sultanate of Oman. *Journal of Geophysical*  
516 *Research* 103, 677-689.

517

518 Platel, J.-P., Roger, J., 1989. Evolution géodynamique du Dhofar (Sultanat d'Oman)  
519 pendant le Crétacé et le Tertiaire en relation avec l'ouverture du golfe d'Aden.  
520 *Bulletin de la Société Géologique de France* 8, 253-263.

521

522 Pouchou, J., Pichoir, J., 1984. "PAP" Z procedure for improved quantitative  
523 microanalysis. *Microanalysis*, 104-106.

524

525 Royer, J.-Y., Chaubey, A.K., Dymant, J., Bhattacharya, G.C., Srinivas, K., Yatheesh,  
526 V., Ramprasad, T., 2002. Paleogene plate tectonic evolution of the Arabian and  
527 Eastern Somali basins. In: Clift, P.D., Kroon, D., Gaedicke, C., Craig, L. (eds). *The*  
528 *tectonic and climatic evolution of the Arabian Sea region*. Geological Society of  
529 London Special Publications 195, 7-23.

530

531 Van Acherbergh, E., Griffin, W.L., Stiefenhofer, J., 2001. Metasomatism in mantle  
532 xenoliths from the Letlhakane kimberlites: estimation of element fluxes. Contributions  
533 to Mineralogy and Petrology 141, 397-414.

534

535 Wells, P.R.A., 1977. Pyroxene thermometry in sample and complex system.  
536 Contributions to Mineralogy and Petrology 62,129-139.

537

538 Witt-Eickschen, G., Seck, H.A., Mezger, K., Eggins, S.M., Altherr, R., 2003.  
539 Lithospheric mantle evolution beneath the Eifel (Germany): 709 constraints from Sr–  
540 Nd–Pb isotopes and trace element abundances 710 in spinel peridotite and  
541 pyroxenite xenoliths. Journal of Petrology 44, 1077–1095.

542

543 Worthing, M.A., Wilde, A.R., 2002. Basanites related to Eocene extension from NE  
544 Oman. Journal Geological Society of London 159, 469-483.

545

546

#### 547 **TABLE CAPTIONS**

548 Table 1. Major (EMPA; wt %) element concentrations for Oman lherzolites and  
549 harzburgites olivines, orthopyroxenes, spinels and clinopyroxenes.  $Mg\# = Mg / (Mg$   
550  $+Fe_{Total}) \times 100$ .

551

552 Table 2. Average REE and trace (LA-ICP-MS; ppm) element concentrations for  
553 clinopyroxenes of Oman mantle xenoliths. (n= number of analysis).

554

#### 555 **FIGURE CAPTIONS**

556

557 Figure 1: Location map of the studied area (after Gnos and Peters, 2003)

558

559 Figure 2: Microphotographs. A: An angular-shaped protogranular harzburgite xenolith  
560 (size of the xenolith: 13 mm x 6 mm); B: porphyroclastic lherzolite, field of view: ~ 6  
561 mm.

562

563 Figure 3: Diagram Cr# ( $100 \times \text{Cr}/(\text{Cr} + \text{Al})$ ) versus Mg# ( $100 \times \text{Mg}/(\text{Mg} + \text{Fe}_{\text{total}})$ ) of spinels of  
564 mantle xenoliths from the North West Al Ashkharah (East Oman) area. Double  
565 crosses: Harzburgites; Crosses: Lherzolites; Filled diamonds: Spitsbergen mantle  
566 lherzolite and harzburgite xenoliths from Ionov et al. (2002); Filled squares in a dark  
567 grey field: mantle peridotite xenoliths from Oman (Nasir et al., 2006); Empty squares  
568 in a light grey field: mantle peridotites from Oman ophiolite from Monnier et al.  
569 (2006).

570

571 Figure 4: Diagrams  $\text{Al}_2\text{O}_3$ ,  $\text{Cr}_2\text{O}_3$  and  $\text{Na}_2\text{O}$  versus Mg# ( $100 \times \text{Mg}/(\text{Mg} + \text{Fe}_{\text{total}})$ ) of  
572 clinopyroxenes of mantle xenoliths from the North West Al Ashkharah (East Oman)  
573 area. Same legend as Figure 3.

574

575 Figure 5: Primitive mantle-normalized REE and incompatible trace element patterns  
576 of the clinopyroxenes characterised by spoon-shaped REE or LREE-enriched  
577 patterns (this study) and from Ionov et al. (2002). See text for explanation.  
578 Normalization values are from McDonough and Sun (1995).

579

580 Figure 6: Primitive mantle-normalized trace element patterns of the clinopyroxenes  
581 from the harzburgite 04OM62B1 and the lherzolite 04OM62B2 (this study) and of the  
582 sample 4-90-1 from Spitsbergen (Ionov et al., 2002). See text for explanation.  
583 Normalization values are from McDonough and Sun (1995).



584

585 Figure 7: Non-modal partial melting modelling for the REE in clinopyroxenes from the  
586 North West Al Ashkharah. The data are normalised to the CI-Chondrite of  
587 McDonough and Sun (1995). Most clinopyroxenes display HREE contents that are in  
588 agreement with a partial melting degree of ~1 to 5%, except for the harzburgite  
589 04OM62b1, for which the HREE cannot be accounted for by a single stage history.

590

591 Figure 8: Diagram  $\text{Cr}_2\text{O}_3$  versus  $\text{Na}_2\text{O}$  of clinopyroxenes of mantle xenoliths from the  
592 North West Al Ashkharah (East Oman) area. Same legend as Figure 3.

593

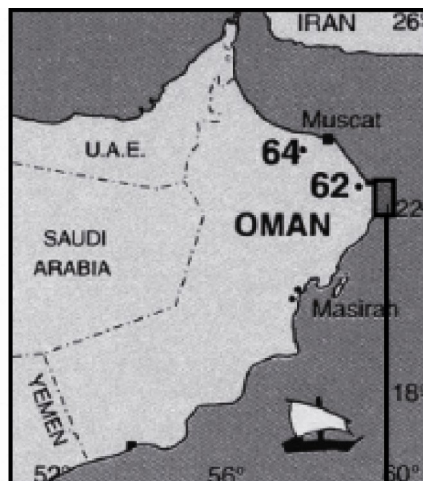
594 Figure 9: Hypothetical melts in equilibrium with clinopyroxene from metasomatised  
595 harzburgites 04OM62b1 and 04OM63c1 compared to the host basanite (Nasir et al.,  
596 2006). Normalising values from McDonough and Sun (1995) and Cpx/basanite  
597 partition coefficients at 0.5 GPa from Adam and Green (2003).

598

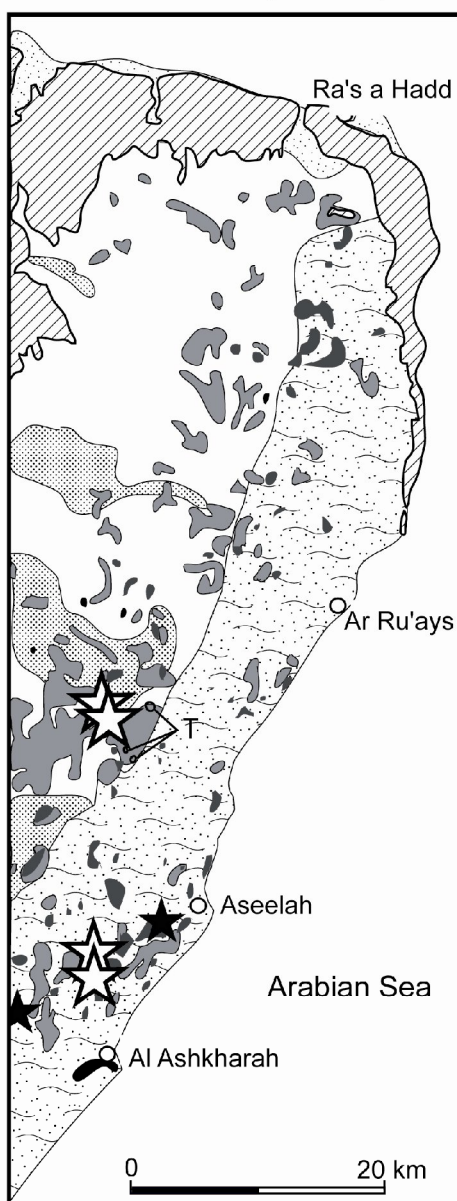
599



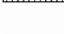

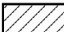
Figure 1

Figure 1





Structural sketch map 1 : 500,000



-  Alluvial fans and terraces
-  Ancient alluvial fans and terraces
-  Sand dunes and Aeolian sand veneer
-  Tertiary volcanics
-  Tertiary - T -

Batain Nappes

-  Sal and Guwaysa Formation
-  Ad Daffah, Aseelah and Qarari Unit

Ophiolite Nappes

-  Ophiolite
-  Studied xenolith localities

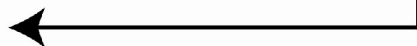


Figure 2

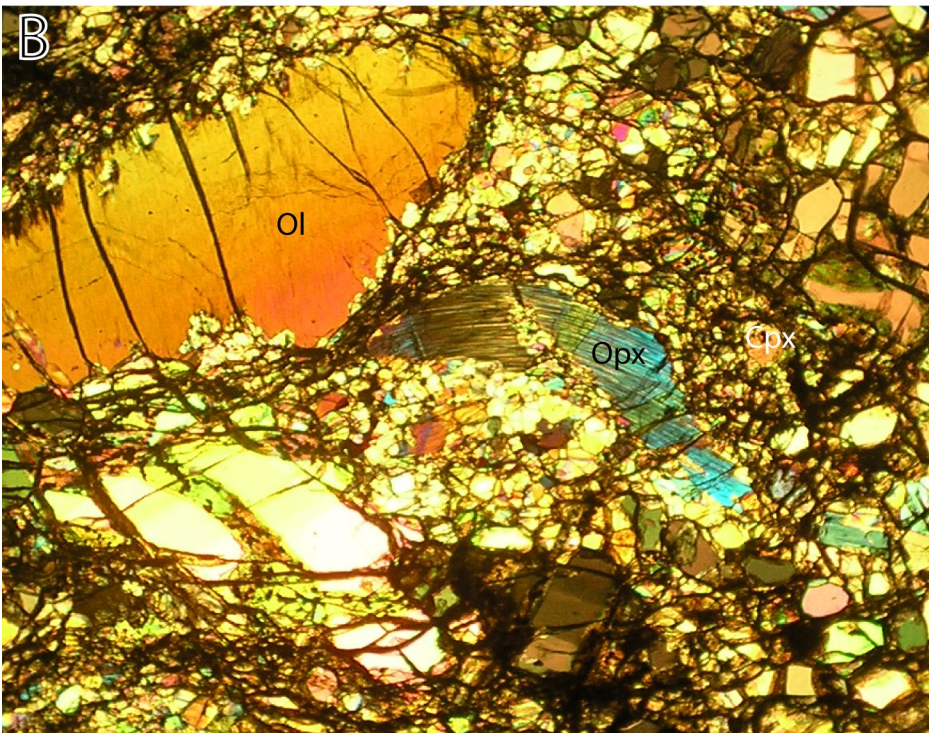
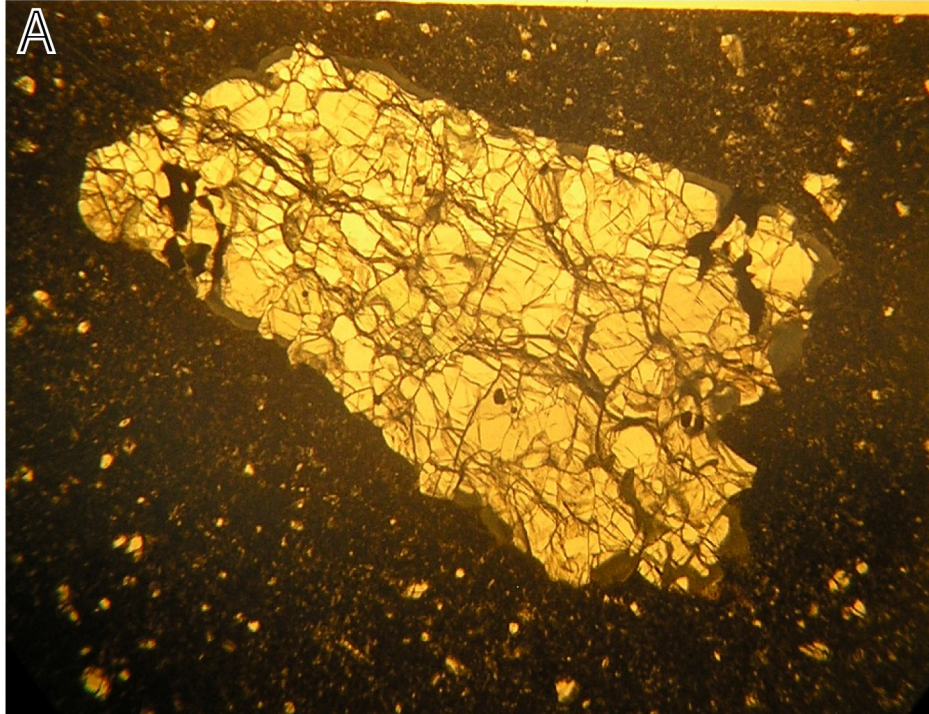


Figure 3

Figure 3

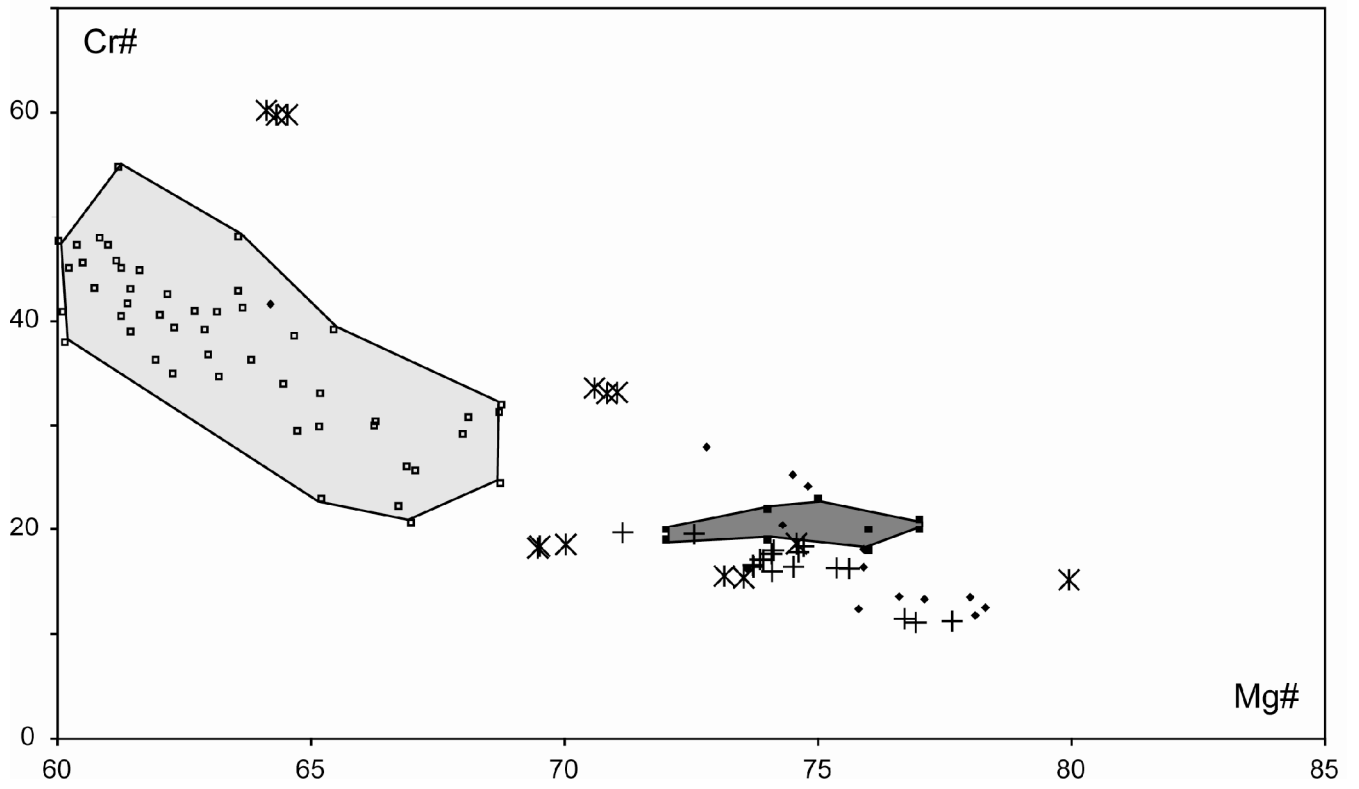


Figure 4

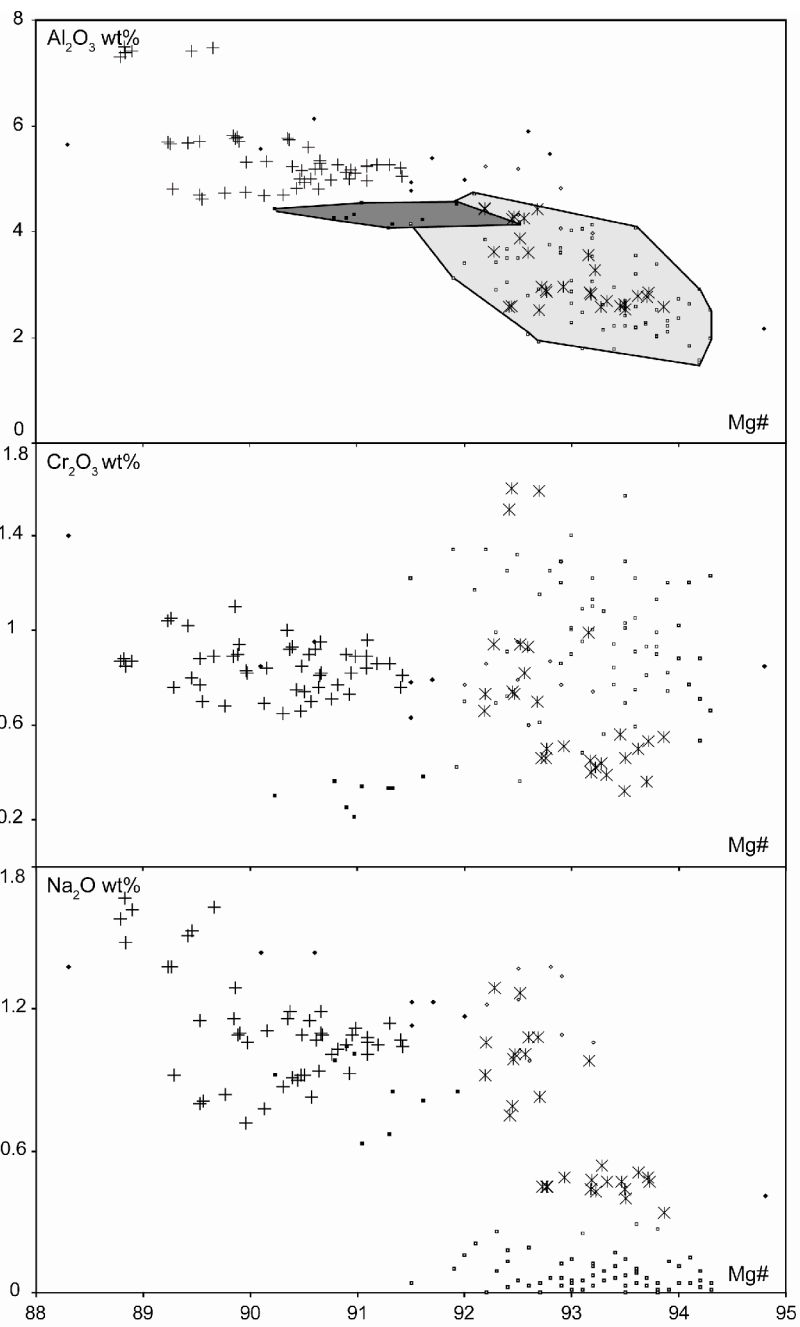


Figure 4

Figure 5

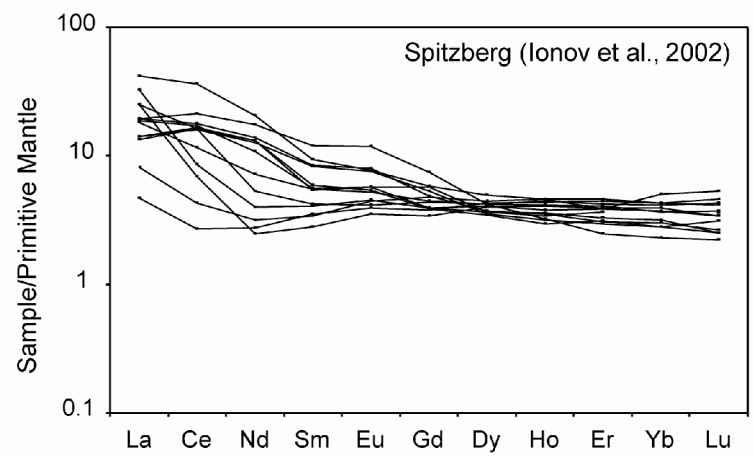


Figure 5

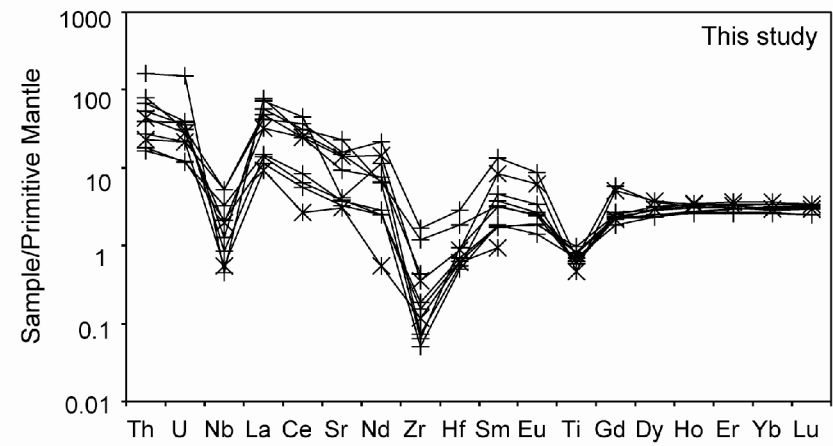
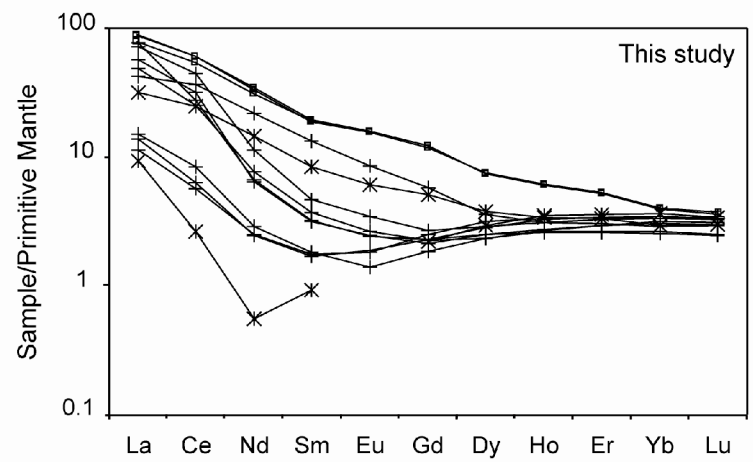
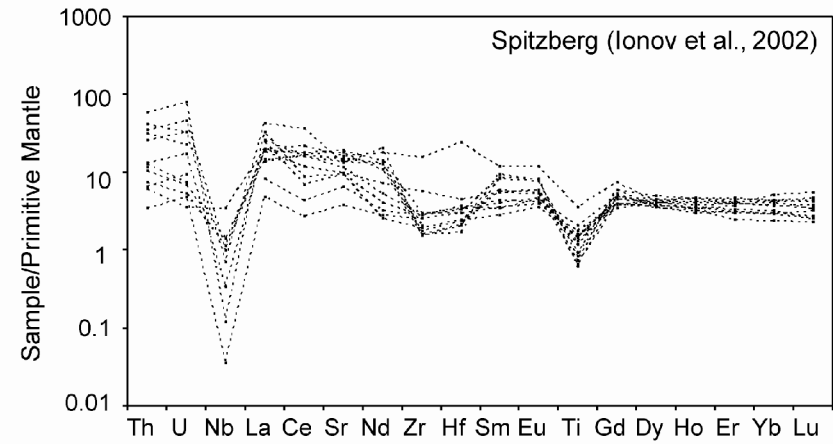


Figure 6

Figure 6

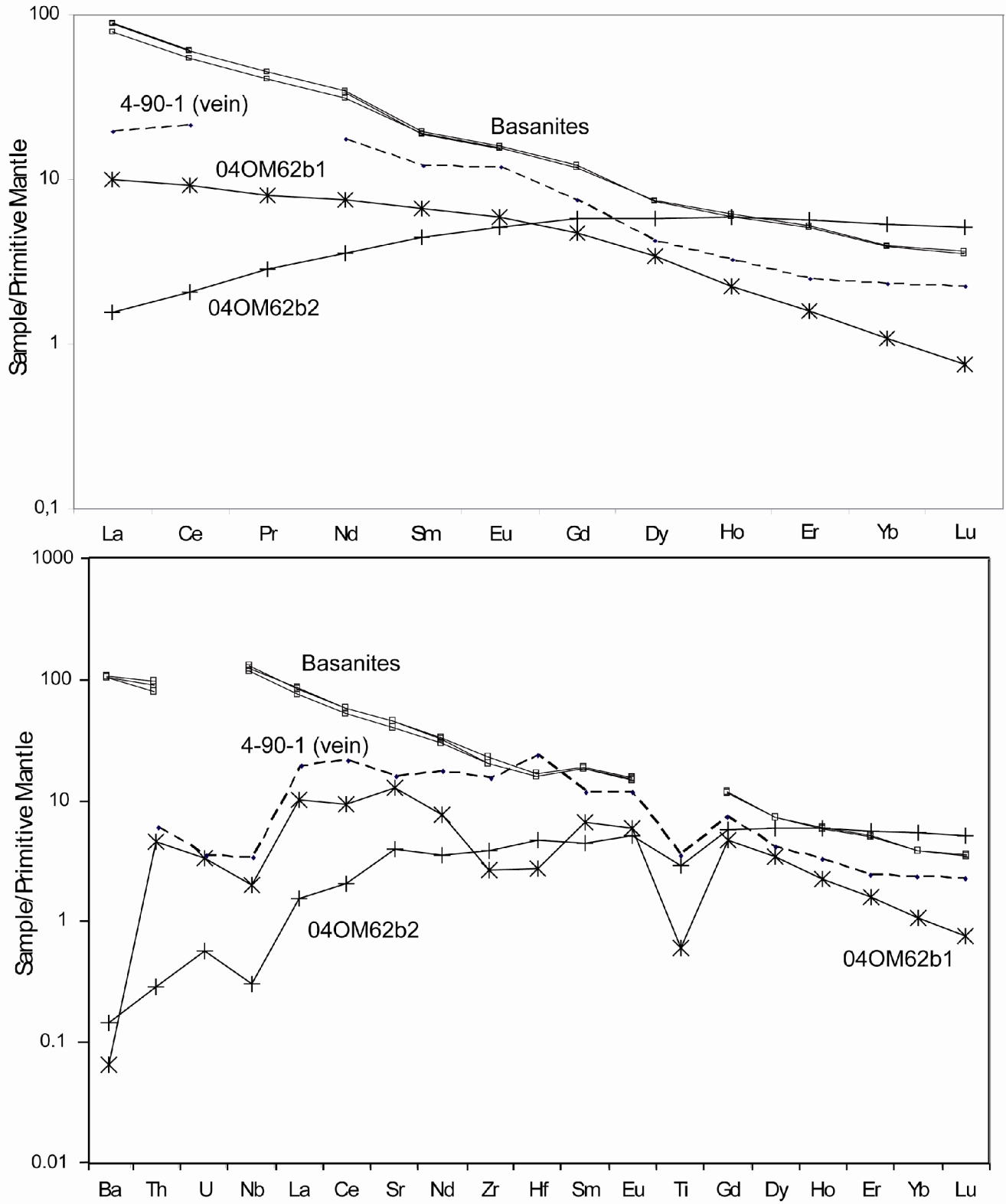


Figure 7

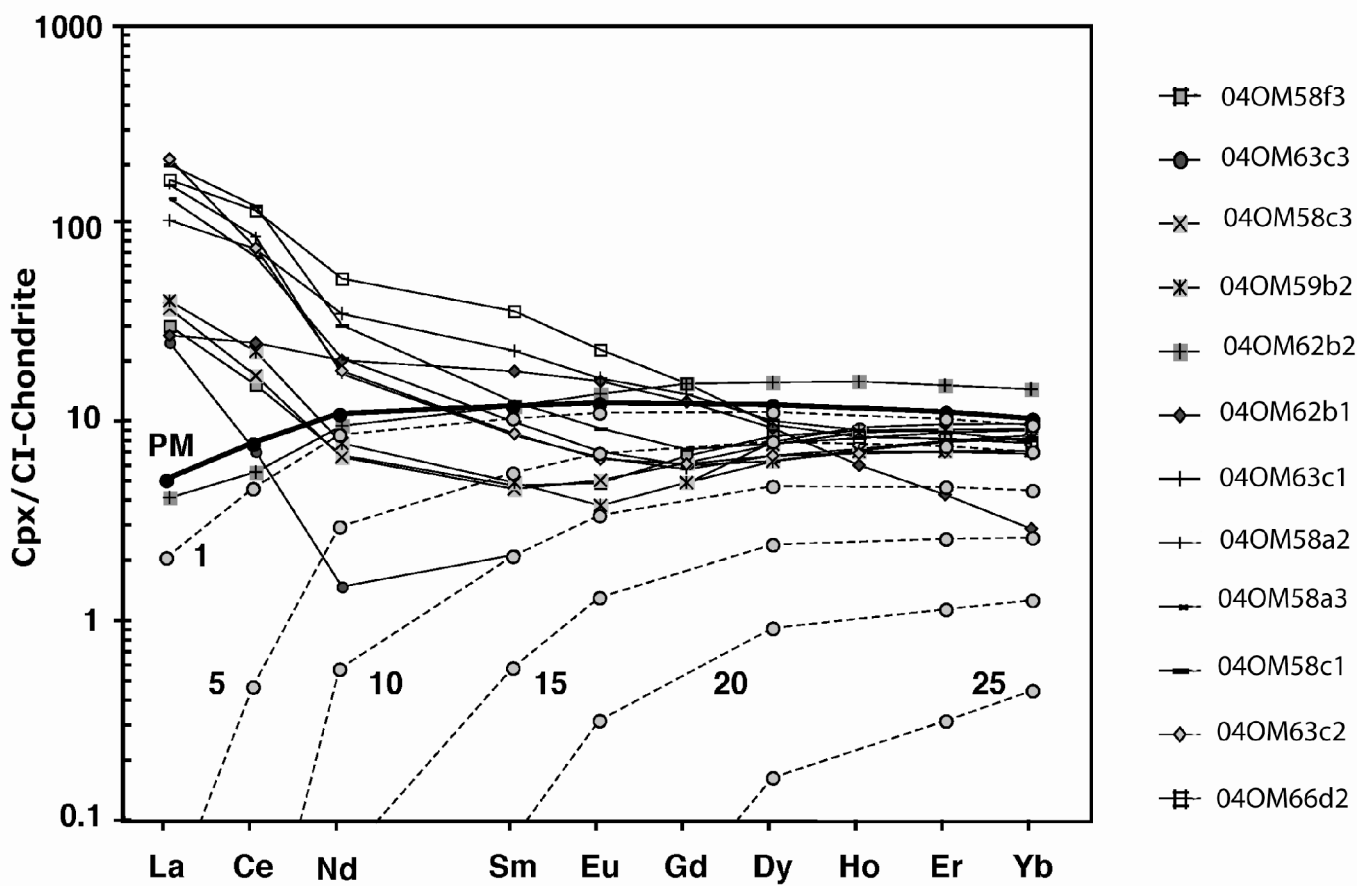




Figure 8

Figure 8

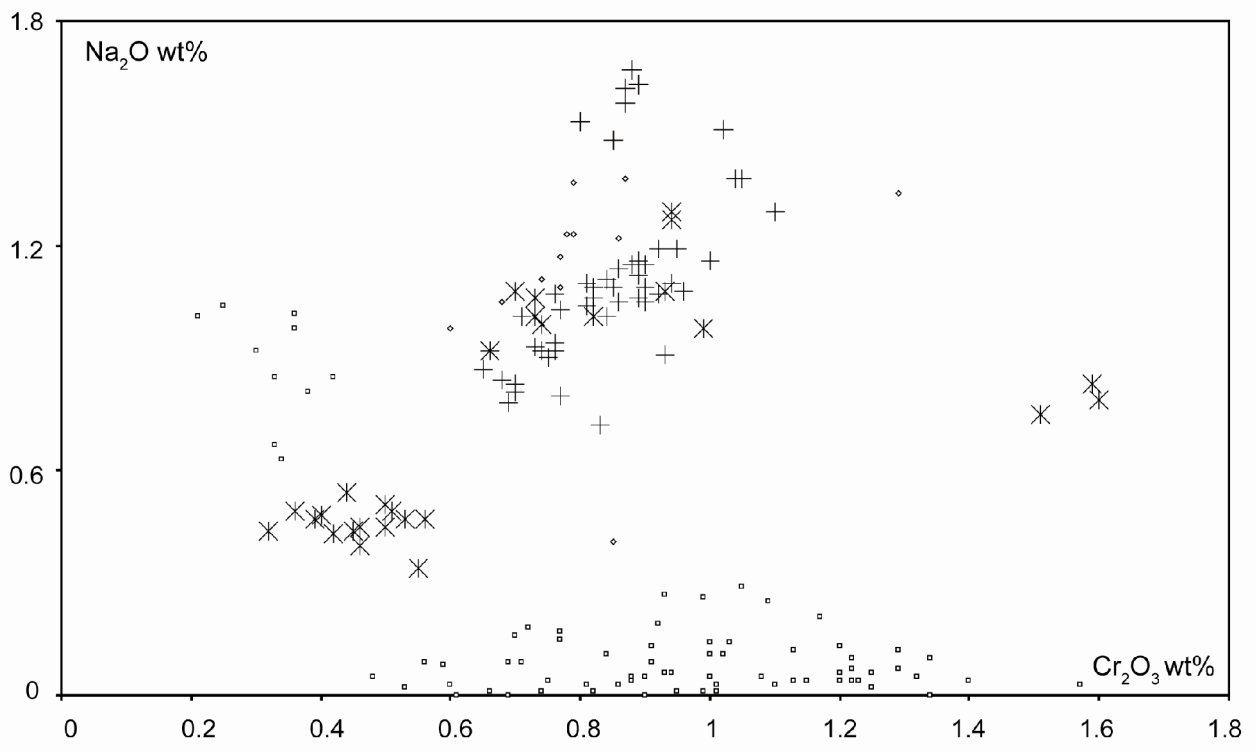


Figure 9

Figure 9

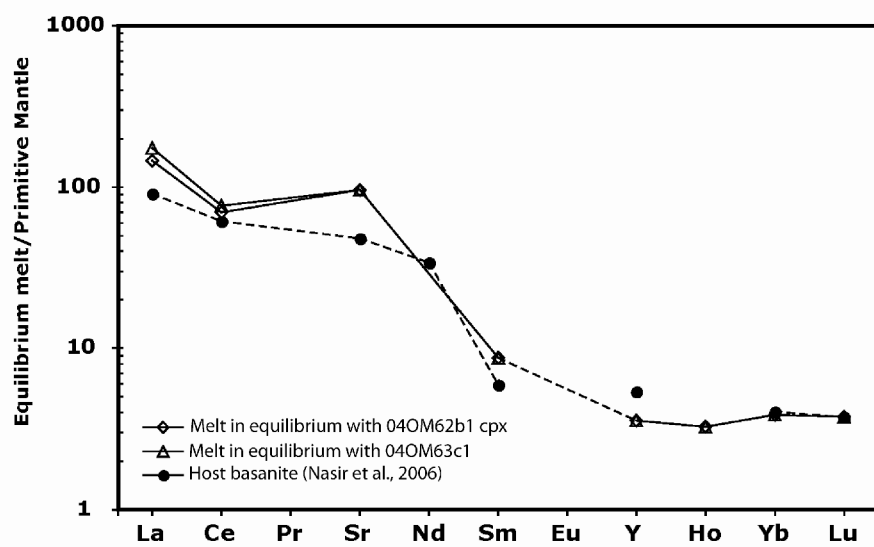




Table 2

[Click here to download Table: Table 2.xls](#)

Clinopyroxene	Harzburgites			Lherzolites								
	04OM63c3	04OM63c1	04OM62b1	04OM58c3	04OM59b2	04OM58f3	04OM62b2	04OM58a2	04OM58a3	04OM58c1	04OM63c2	04OM66d2
	n=4	n=3	n=3	n=5	n=3	n=3	n=4	n=5	n=4	n=4	n=3	n=3
Sc	97	91	63	76	69	70	68	71	62	97	55	66
Ti	945	569	722	1008	851	1154	3482	950	755	701	718	846
V	244	243	181	232	246	222	258	241	244	287	186	258
Ni	403	310	381	270	291	300	324	364	317	318	262	311
Rb	0.80	0.80	bdl	bdl	bdl	1.55	bdl	1.00	0.62	0.26	0.66	1.86
Sr	61	273	254	76	75	65	79	456	183	83	296	313
Y	14	14	4	12	12	14	24	13	13	13	10	13
Zr	1.23	3.69	28	1.63	0.52	1.98	40	0.68	4.58	0.76	12	18
Nb	0.38	1.34	1.36	0.59	2.23	1.44	0.21	0.88	3.61	bdl	0.30	3.56
Ba	1.34	1.66	0.43	0.34	0.61	0.44	0.96	1.55	0.52	0.40	0.74	7.4
La	6.0	25	6.5	8.9	9.7	7.3	1.00	37	32	47	50	39
Ce	4.41	46	15	11	14	9.5	3.49	53	42	75	46	71
Pr	0.18	4.92	2.03	0.95	1.20	0.87	0.73	3.61	3.33	5.9	3.26	7.1
Nd	0.69	16	9.4	3.08	3.63	3.16	4.43	8.0	9.63	14	8.4	24
Sm	0.32	3.40	2.69	0.69	0.75	0.72	1.80	1.29	1.50	1.89	1.31	5.38
Eu	bdl	0.94	0.91	0.29	0.22	0.28	0.79	0.38	0.41	0.53	0.37	1.32
Gd	0.99	2.78	2.56	1.26	1.00	1.36	3.13	1.17	1.22	1.47	1.24	3.15
Dy	1.98	2.53	2.32	1.96	1.58	2.13	3.94	1.69	1.59	1.95	1.69	2.42
Ho	0.52	0.50	0.34	0.49	0.39	0.50	0.88	0.41	0.40	0.46	0.38	0.47
Er	1.58	1.45	0.70	1.48	1.16	1.49	2.48	1.30	1.29	1.44	1.15	1.34
Yb	1.59	1.30	0.48	1.51	1.17	1.48	2.38	1.40	1.35	1.48	1.13	1.28
Lu	0.23	0.20	0.05	0.23	0.17	0.22	0.34	0.21	0.20	0.23	0.17	0.20
Hf	0.17	0.25	0.77	0.18	0.14	0.20	1.34	0.27	bdl	0.16	0.53	0.82
Th	1.82	3.45	0.36	3.12	1.44	1.29	0.02	4.28	6.31	5.32	13	2.17
U	0.44	0.57	0.07	0.77	0.24	0.25	0.01	0.72	0.64	0.81	3.12	0.44

bdl: below detection limit